# Snapshot circular dichroism measurements

Oriol Arteaga, Zoubir El-Hachemi, Razvigor Ossikovski

Research Article | Vol. 27, No. 5 | 4 Mar 2019 | OPTICS EXPRESS 6746
Optics EXPRESS

# Snapshot circular dichroism measurements

ORIOL ARTEAGA,[1,2,*] ZOUBIR EL-HACHEMI,[3] AND RAZVIGOR OSSIKOVSKI[2]

[1]*Departament de Física Aplicada, IN2UB, Universitat de Barcelona, 08028 Barcelona, Spain*
[2]*LPICM, CNRS, École Polytechnique, 91128 Palaiseau, France*
[3]*Departament de Química Inorgànica i Orgànica, IEEC-UB, Universitat de Barcelona, 08028 Barcelona, Spain*
[*]*oarteaga@ub.edu*

**Abstract:** Two coherent waves carrying orthogonal polarizations do not interfere when they superpose, but an interference pattern is generated when the two waves share a common polarization. This well-known principle of coherence and polarization is exploited for the experimental demonstration of a novel method for performing circular dichroism measurements whereby the visibility of the interference fringes is proportional to the circular dichroism of the sample. Our proof-of-concept experiment is based upon an analog of Young's double-slit experiment that continuously modulates the polarization of the probing beam in space, unlike the time modulation used in common circular dichroism measurement techniques. The method demonstrates an accurate and sensitive circular dichroism measurement from a single camera snapshot, making it compatible with real-time spectroscopy.



## 1. Introduction

Circular dichroism (CD) is the differential absorption of circularly polarized light. Despite this differential absorption being typically very small in optically active enantiomers ($10^{-5}$–$10^{-4}$), CD spectroscopy has become a well-established technique, especially as a method for identifying structural motifs in chiral proteins [1]. Due to its intrinsic weakness, the detection of CD requires relatively complex and expensive instruments that often need to integrate the low signal over significant measurement time.

Modern approaches to CD measurement are based on a polarization-modulation scheme in which linearly polarized probing light passes through a quartz crystal that has been subjected to periodic time-varying mechanical stress inducing birefringence due to the photoelastic effect. The modulation device, commonly called photoelastic modulator, produces circular polarizations with alternating handedness in time [2]. In the early realizations of spectroscopic CD measurements from 1960's [3], the polarization modulation was also accomplished with electrically driven Pockels cells, but nowadays virtually all commercial CD instruments use photoelastic modulators. Regardless whether Pockels cells or photolastic modulators are used as polarization-modulation elements, the measurement approach based on the analysis of the temporal variation of the polarization of the modulated probing light is the same.

In this work we present a novel method for spectroscopic CD characterization that is based on spatial rather than on temporal polarization modulation. The application of multi-domain spatial, spectral, angular, etc modulation approaches has been previously explored by Tyo and coworkers in the more general context of polarimetry [4, 5]. In our method, different points of the sample are illuminated with different, well-controlled states of polarization with alternating handedness. The presence of CD in the sample results in the formation of a periodic interference pattern at the detector. As chiroptical data are obtained from the analysis of a single snapshot of the interference pattern, the novel approach is not subject to measurement time constraints typical of the temporal modulation approaches. Therefore, it can be expected to be suitable, for

#351286 https://doi.org/10.1364/OE.27.006746
Journal © 2019 Received 7 Nov 2018; revised 7 Jan 2019; accepted 8 Jan 2019; published 22 Feb 2019

Optics EXPRESS

example, for the study of ultrafast conformational changes in biomolecules. Indeed, the major measurement-time-limiting component in conventional CD spectrometers is the photoelastic modulator which usually runs at 50 kHz. Since the acquisition of several modulation periods of the signal is necessary, the measurement time of these instruments is typically larger than about 1 ms.

The use of spatial modulation in a polarized light beam has been previously considered in Stokes polarimetry using polarization gratings [6], Savart plates [7,8] and wedge prisms [9]. Also in the context of Stokes polarimetry, methods have been developed to encode both polarization and wavelength information in the spatial dimension [10–12]. To our knowledge only polarization gratings have been previously considered for CD detection, as these optical components produce positive and negative diffraction orders of opposite handedness [13–15] and even a complete Mueller matrix polarimeter has been theoretically proposed with them [16]. The method we propose is not based on diffraction orders but rather on the coherent superposition of two beams with orthogonal polarizations, that results in an spin-dependent redistribution of light intensity in the transverse plane. It uses a thin doubly refracting crystal slab as a key optical element creating an analog of Young's double-slit experiment [17] according to the well known interference-polarization laws of Fresnel and Arago [18–20]. In what follows we describe the principle of operation of the novel technique, as well as its proof-of-concept spectroscopic implementation in the form of a simple, low-cost setup capable of measuring CD and we compare it with conventional instruments using the time-modulation approach.

## 2. Principle of operation

In our proposed experiment a partially coherent light beam is sent through a thin slab of crystal calcite. The optic axis of the uniaxial crystal makes an angle of 45° with the facets of the slab and separates the photons by their polarization due to the well-known double refraction phenomenon; see Fig. 1. Consider an incident beam polarized at 45° with respect to the $yz$ plane of the laboratory reference frame shown in Fig. 1. Double refraction in the crystal splits the beam into two rays, called ordinary and extraordinary, that follow slightly different paths. Due to the initial 45° linear polarization of the incident beam, the ordinary and extraordinary emerging beams have the same intensity; their polarizations are, respectively, horizontal (along the $x$ axis) and vertical (along the $y$ axis). The two beams, spatially separated by the small distance $d$ upon exiting the crystal, can be partially recombined if made slightly divergent (for example, by using a lens that focuses the incident beam on the entrance facet of the crystal).

The spatial modulation of the polarization state of the coherently recombined beam arises because the slightly divergent ordinary and extraordinary beams forming the latter have generally traveled different pathlengths before reaching a point on the $y$ axis. The pathlength difference results in a phase difference –or retardation– between the horizontal and vertical polarizations of the ordinary and extraordinary beam components, thus giving rise to a generally elliptical polarization state for the recombined emerging beam. The spatial polarization pattern varies periodically between left- and right-handed circular polarizations while passing through 45° and -45° linear polarization states and, most generally, through orthogonal elliptical states; see Fig. 2. The two pathlengths being the same along the $x$ axis, there is no polarization modulation along it. Therefore, the doubly refracting crystal acts as a spatially varying retarder. This effect has been recently studied experimentally in [17]. The calculation reported in the appendix section shows that the doubly refracting crystal is described by the Mueller matrix of a horizontal linear

Optics EXPRESS

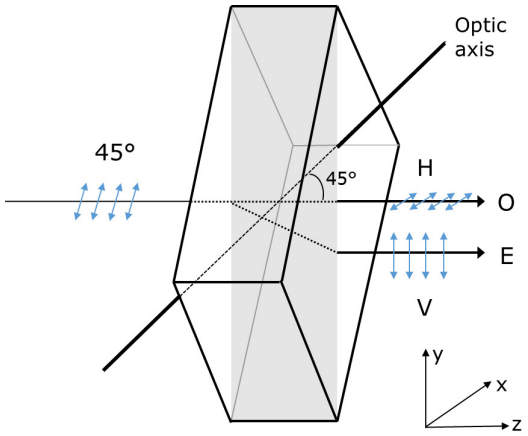


Fig. 1. **Double refraction in calcite**. The incident beam, linearly polarized at 45°, is split into ordinary (O) and extraordinary (E) beams. The grayed area indicates the $yz$ plane of the laboratory reference frame containing the two beams and the optic axis of calcite. The polarization of the ordinary beam, orthogonal to this plane, is horizontal (H), i.e. is directed along the $x$ axis. The polarization of the extraordinary beam, contained in the plane in question, is vertical (V), i.e. is directed along the $y$ axis.

retarder,

$$\mathbf{M}_R = \begin{pmatrix} 1 & 0 & 0 & 0 \\ 0 & 1 & 0 & 0 \\ 0 & 0 & \cos\phi(y) & -\sin\phi(y) \\ 0 & 0 & \sin\phi(y) & \cos\phi(y) \end{pmatrix}, \tag{1}$$

The retardation $\phi(y)$ varies along the vertical (y) axis since it directly depends on the phase difference arising from the difference in optical paths of the ordinary and extraordinary beams upon traveling from the crystal to the measurement point, as explained above. Note that when $\phi$ is zero or a multiple of $2\pi$ the Mueller matrix equals the identity while, for other values, it continuously evolves between that of a horizontal quarter-wave plate ($\phi = -\pi/2$), a vertical quarter-wave plate ($\phi = \pi/2$), and a half-wave plate ($\phi = \pi$). Therefore, in our method, the spatial separation of the ordinary and extraordinary beams due to the double refraction phenomenon leads, after coherent superposition of the beams, to a spin (circular polarization) modulation along the $y$ axis as shown in Fig. 2.

The doubly refracting crystal configuration is, in fact, analogous to the classic Young's double-slit experiment in which orthogonal polarizers have been placed after the slits [20]. Indeed, the two emerging ordinary and extraordinary beams, spatially separated upon exiting the crystal slab, act as two coherent light sources exactly as the two orthogonally polarized slits in Young's double-slit experiment. No interference fringes are seen on the detection screen because beams with orthogonal polarizations do not interfere. However, if, for example, a 45° linear polarizer is placed between the crystal slab and the detector, horizontal periodic interference fringes will appear. This can be easily understood by observing the polarization modulation pattern of Fig. 2: dark horizontal fringes arise whenever the transmission axis of the polarizer is orthogonal to the azimuth of the linear polarizations shown in the pattern. Similarly, a fringe pattern will appear for the preferential absorption of one handedness of the circular polarization. Therefore, a sample exhibiting CD will also entail the formation of a horizontal fringe pattern.

Optics EXPRESS

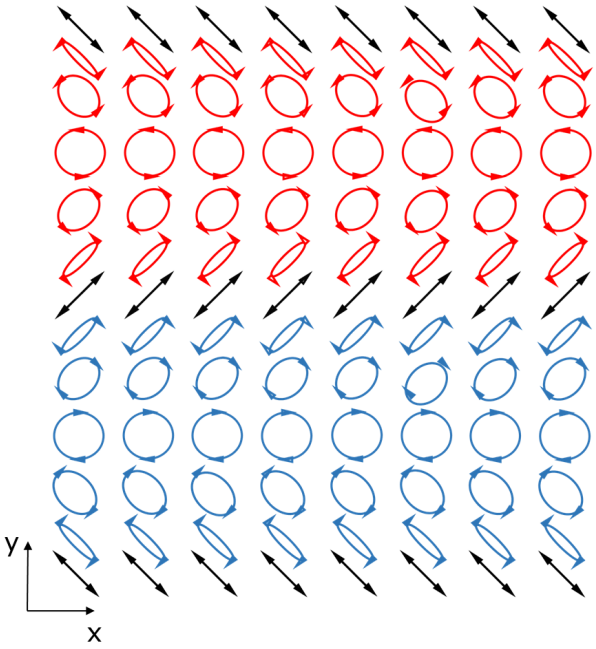


Fig. 2. **Spatially modulated polarization pattern across the emerging beam area**. Red and blue colors denote opposite handedness. The polarization modulation is periodic along the vertical ($y$) axis; there is no modulation along the horizontal ($x$) axis.

The best fringe contrast (the highest visibility) is obtained by the insertion of a 45° or -45° linear polarizer, because it will block completely the linear polarization states normal to its transmission axis (creating dark fringes) and will transmit those parallel to the latter (generating white fringes). The situation will be exactly the same with a left or right circular polarizer: it will completely block the polarizations of opposite handedness and will let pass the ones having the same handedness, thus ensuring best possible fringe contrast. A sample exhibiting CD behaves like a very weak partial (left or right) circular polarizer: the fringe contrast will be significantly lower, in most occasions detectable only after Fourier analysis of the acquired images, as discussed in the next section.

The distance between two successive fringes (the period of the fringe pattern) is given by

$$\Delta x = D\lambda/d, \tag{2}$$

where $\lambda$ is the wavelength, $d$ is the separation between the ordinary and extraordinary beams at the exit facet of the crystal (see Fig. 1) and $D$ the distance from the crystal to the detection screen. The period of the fringes, $\Delta x$, changes with the wavelength not only because it directly depends on $\lambda$ but also because the separation of the beams $d$ depends on the dispersive nature of the crystal birefringence. As $d$ increases with the birefringence in the UV range typically, this results in higher spatial frequency - or shorter period - of the fringes in this spectral region.

## 3. Proof-of-concept experiment

Our proposed experiment requires probing light with a certain degree of coherence. Certainly, laser light sources are suitable for its implementation and, as the technique itself poses no limitations on the detection time, it is fully compatible with ultrashort pulses. For example, owing to the availability of femtosecond laser sources, several femtosecond time-resolved

Optics EXPRESS

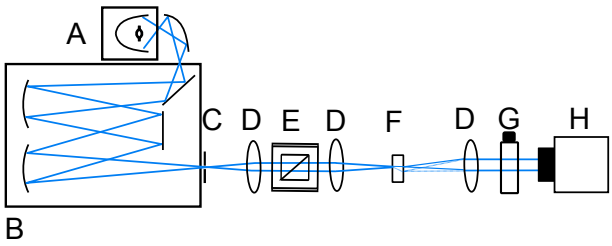


Fig. 3. **Schematics of the experimental system**. A, light source; B, monochromator; C, pinhole; D, lenses; E, 45° polarizer; F, doubly refracting crystal; G, sample; H, camera.

chiroptical experiments have been recently proposed [21–24], albeit at the sacrifice of the polarization modulation that our method preserves. However, in most research and industry laboratories circular dichroism is essentially considered as a spectroscopic technique because single wavelength measurements are usually not sufficiently informative. Consequently, in our initial demonstration of the technique we decided to keep the light source most commonly used for CD spectroscopy namely, a broadband 75W Xe arc lamp with rather limited coherence.

The schematics of proof-of-concept experimental setup is given in Fig. 3. The basic optical layout (disregarding lenses) is identical to that of conventional CD spectrometers, the only difference being the doubly refracting crystal slab replacing the photoelastic modulator. The broadband light of the Xe lamp is monochromatized with a monochromator (Horiba iHR 320) and passes trough a pinhole of 300 nm of diameter. The monochromator and the pinhole serve, respectively, to increase the temporal and the spatial coherence of the beam. Because of the moderate coherence length of the Xe lamp, widening the monochromator slits or removing the pinhole strongly decrease the visibility of the fringes.

The degree of coherence of the probing light can be experimentally evaluated from the visibility of the fringes as we shall see in the next section. In general, the latter is strongly affected by the thickness of the doubly refracting crystal slab and further depends on the wavelength of light. Thick crystals result in large $d$ values which, in turn, give rise to significant optical path differences over which coherence needs to be preserved in order for the fringes to be visible. To avoid such situations, we use a relatively thin calcite crystal (thickness of 1.2 mm) creating a beam separation $d \simeq 0.13$ mm at the wavelength of 550 nm.

We use a low-cost conventional camera (Flir-Point Grey GS3-U3-32S4M-C) as imaging detector. It senses light in the wavelength range 350 – 900 nm; its best quantum efficiency lies within the 450 – 650 nm interval. This camera, while quite suitable for visible CD spectroscopy, does not allow for UV measurements. The UV region is a very important spectral range in CD spectroscopy because many electronic CD bands of organic compounds appear at wavelengths below 300 nm. However, as there are image sensors with good UV performance on the market, it should not be a problem to extend our method to that range. The camera acquires full frame 2048×1535 pixel images and these are Fourier-analyzed columnwise (i.e. along the $y$ direction in Fig. 2). According to the calculation given in the appendix, the detected intensity at each pixel of any of the 1535 column arrays is given by

$$I(y) = (m_{00} + m_{02}\cos\phi(y) + m_{03}\sin\phi(y))I_0, \tag{3}$$

where $m_{ij}$ are elements of the Mueller matrix of the sample, $I_0$ is the probing light intensity and

$$\phi(y) = \frac{2\pi d}{\lambda D}y. \tag{4}$$

By applying Fourier analysis the intensity signal can be separated into its DC and AC components,

Optics EXPRESS

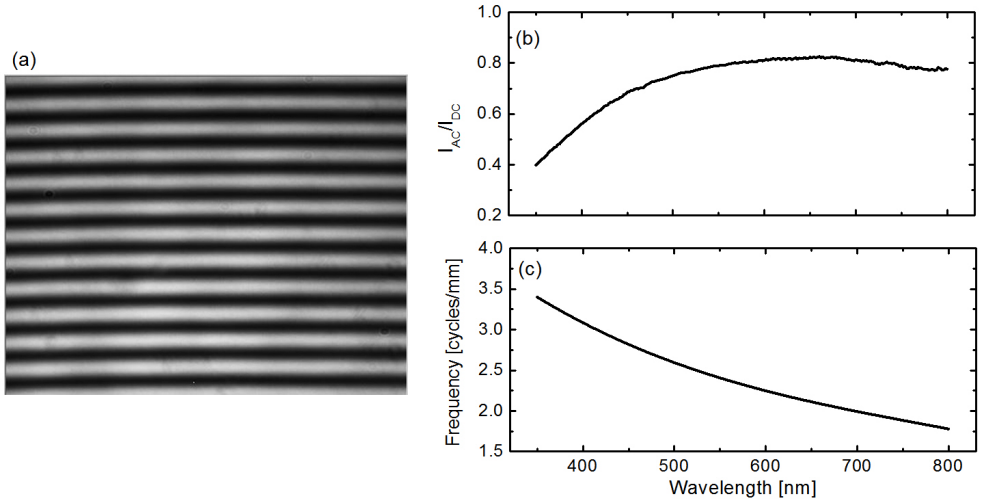


Fig. 4. **Calibration results.** a, horizontal fringe pattern obtained with the calibration 45° polarizer. b, spectral dependence of the ratio $I_{AC}/I_{DC}$. c, spatial frequency (in cycles/mm) of the fringe pattern.

$$I_{DC} = I_0 m_{00}, \tag{5a}$$

$$I_{AC} = I_0 \sqrt{m_{02}^2 + m_{03}^2}. \tag{5b}$$

In an isotropic sample $m_{02} = 0$ and the ratio $I_{AC}/I_{DC}$ will then measure the CD of the sample, since $m_{03}/m_{00} \simeq$ CD, as it will be discussed later. Note that the ratio in question is not affected by possible intensity fluctuations of the light source ($I_0$). Note also that to obtain a measurement of $I_{AC}/I_{DC}$ a single column of pixels is sufficient, in principle. The use of the whole sensor area permits efficient signal averaging that greatly improves the signal-to-noise ratio. The sign of CD can be obtained from the phase term of the Fourier analysis, taking as a phase reference a sample with known signs of $m_{02}$ and $m_{03}$ Mueller matrix elements, for example, a linear polarizer at 45° ($m_{02} = 1$ and $m_{03} = 0$).

In photoelastic-modulator-based CD instruments the ratio $I_{AC}/I_{DC}$ is obtained after determining the AC component of the signal by using synchronous detection (based on a lock-in amplifier) with a reference frequency from the photoelastic modulator. In our interferometry-based technique the role of reference frequency is played by the spatial frequency given by the factor standing in front of $y$ in Eq. (4). The value of the spatial frequency depends on the optical configuration of the experimental setup – through the two parameters $d$ and $D$; see Eq. (4) – as well as on the wavelength $\lambda$ of the probing light. It can be determined spectroscopically through calibration.

## 4. Calibration and evaluation of coherence

The degree of coherence of the light superposition process that generates the spatial modulation pattern in Fig. 2 can be evaluated by using a polarizer as calibration sample. When the polarizer transmission axis is oriented at 45° or -45°, a clear interference pattern is detected by the camera (see an experimental example of such pattern in Fig. 4(a)). In an ideal situation with fully coherent illumination the polarizer would exhibit a ratio of $|I_{AC}/I_{DC}| = 1$. This ratio describes the contrast between the bright and dark interference regions and therefore, accounts for the visibility of the fringes. The visibility value would fall to zero when the pathlength difference between the ordinary and extraordinary rays exceeds the coherence length of the probing light.

Optics EXPRESS

The spectral dependence of the visibility for our experimental setup is shown in Fig.4(b). The measured ratio strongly depends on experimental conditions such as the slit width of the monochromator, the pinhole diameter and the thickness of the doubly refracting crystal. The drop at shorter wavelengths (below 500 nm) is mostly due to the increased birefringence of calcite leading to a larger separation ($d$) of the emerging beams and thus, requiring higher coherence to maintain the same visibility. The measured visibility peaks at around 0.82 which, although sufficiently high, is still somewhat below the theoretical maximum (the unit). This value is indicating the attainable coherence limit of our setup since reducing the pinhole diameter or decreasing the monochromator slit width does not increase it any further. Probably, we cannot reach a value closer to the theoretical maximum because of the limited performance of the camera in detecting black and bright levels.

The calibration is also used to determine the reference spatial frequency of the experiment (Fig. 4(c)). This frequency corresponds to the number of cycles (fringes) per unit length across the vertical (y) axis of the camera sensor. The value of the spatial frequency depends on the thickness of the doubly refracting crystal, the wavelength of the probing light and the optical layout of the setup, but once these parameters are fixed it is a constant, characteristic parameter of the instrument. Figure 4(c) shows the strong spectral dependence of the spatial frequency. Here the the $1/\lambda$ response is dominant, in full agreement with Eq. (4), because in this spectral range the chromatic variation of calcite's birefringence – and therefore, of the beam separation $d$ – is not significant [25].

To properly measure weak CD signals it is necessary to do a baseline correction using a background spectrum obtained without sample. In our method, baseline offsets are mostly affected by the alignment of the double refracting crystal and the homogeneity of the illumination across the camera sensor. Baseline corrections are also routinely made in PEM-based CD instruments as, for example, one of the factors that can cause a baseline drift is the temperature sensitivity of the PEM.

## 5. CD measurement

For an isotropic sample exhibiting CD the ratio $I_{AC}/I_{DC}$ can be written as

$$\frac{I_{AC}}{I_{DC}} = \frac{m_{03}}{m_{00}} = \tanh \mathrm{CD}, \tag{6}$$

according to the parameterization of a Mueller matrix corresponding to a homogeneous chiral medium [26, 27]. Recall that CD is defined phenomenologically as

$$\mathrm{CD} = 2\pi(k_- - k_+)l/\lambda, \tag{7}$$

where $k_-$ and $k_+$ are, respectively, the extinction coefficients for left- and right circular polarization and $l$ is the pathlength of light in the medium. As CD is typically very small, $\tanh \mathrm{CD} \simeq \mathrm{CD}$. Commercial instruments do no measure circular dichroism according to the expression in (7), but rather in terms of ellipticity ($\theta$) which is related to CD through $\theta = \mathrm{CD}/2$, $\theta$ being usually expressed in millidegrees (mdeg).

To illustrate our method we measured a nickel tartrate solution that features CD bands within the spectral range of our experimental setup. It was prepared by mixing 0.24 M nickel sulfate solution and 0.36 M sodium potassium tartrate solution with a 1:1 volume ratio. Figure 5 shows the results of the CD measurements (in units of ellipticity) of the nickel tartrate solution in a 10-mm pathlength cuvette after baseline correction. For comparison, we performed the measurements with two calcite crystal slabs having different thicknesses. For a probing light with given spatial and temporal coherency, thinner slabs allow measurements at shorter wavelengths since they feature a smaller separation between the ordinary and the extraordinary beams.

Optics EXPRESS

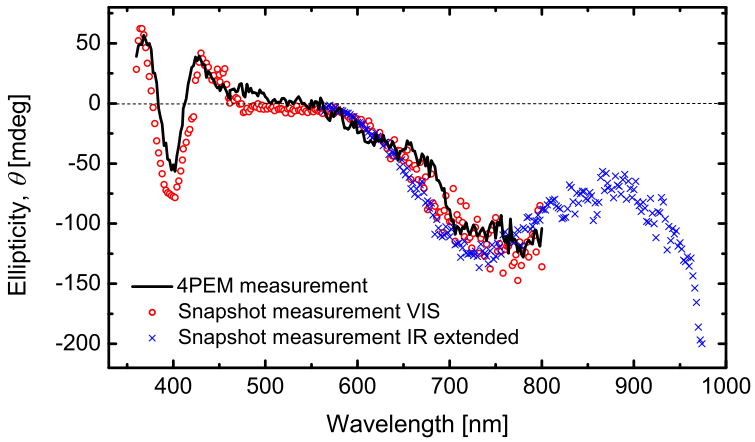


Fig. 5. **CD spectrum of nickel tartrate solution**. The graph compares three different measurements. The 4PEM measurement (solid line) was made with the instrument described in [28], while the scattered points correspond to the snapshot method. The UV-visible-range measurement was made using a crystal with a thickness of ~ 1.2 mm, while the near-IR-extended one was obtained with a ~ 2.0-mm-thick crystal.

However, they may become unsuitable at longer wavelengths if the spatial frequency is so low that not enough periods of fringes are collected. Figure 5 also presents, for comparison, the temporal-modulation-based CD measurement on the same sample obtained with a home-made four-photoelastic-modulator (4-PEM) instrument described in detail in [28].

The spatial modulation method requires the CD properties of the medium to be homogeneous across the illuminated area of the sample. In practice, this condition is met for all CD measurements performed on solutions.

Our proof-of-concept experiment demonstrates that the novel method for CD measurements is viable and of easy use, even for spectroscopic measurements. We anticipate that more advanced experimental implementations of this method will largely surpass the capabilities shown by our first experiment and will extend the spectral range to the UV, which typically is the spectral region of interest for biological samples. In future implementations, we suggest using a monochromatic or broadband light source with superior coherence properties (e.g., a laser, a laser-driven light source, or a supercontinuum laser). By using a pulsed-light source one could also increase the time resolution well beyond the exposure time of the detector. Other experimental improvements that can be anticipated involve modifying the optical layout by using mirrors instead of lenses to maximize the light throughput, as well as employing a high-end low-noise camera.

## 6. Conclusion

We have presented a novel snapshot method for the measurement of CD. The technique is based on the spatial polarization modulation of the probing light achieved with a doubly refracting crystal implemented in an optical configuration that is an analog of the classic Young's double-slit interference experiment. A single snapshot of the formed interference pattern allows for the determination of the CD of the sample, the visibility of the fringes being proportional to it.

We have described a practical implementation of the novel technique in a simple, low cost spectroscopic setup capable of detecting CD with remarkable sensitivity in the visible range and we have compared the result with that of polarimeter instrument based on temporal polarization modulation. We believe that more refined implementations of the method described may potentially surpass the sensitivity of conventional CD spectrometers and may hugely improve

Optics EXPRESS

their temporal resolution. The novel snapshot CD technique, not subjected to the constraints of temporal polarization modulation, opens the way to measuring conformational changes of biomolecules in real time.

## A. Appendix: Calculation of the detected intensity

The intensity at every pixel of the detector, $I(x, y)$, where $x$ and $y$ respectively refer to the horizontal and vertical pixels in the laboratory reference frame (see Fig. 1) is found from the coherent superposition of the ordinary and extraordinary beams, produced by the birefringent crystal, that interact with the sample before reaching the detector.

The Stokes-Mueller formalism is typically used to evaluate the evolution of the light intensity in polarimetric setups. However, this formalism cannot directly deal with coherent superposition processes such as the one taking place in our method. To handle such processes, one must start with the coherent Jones formalism and then switch to the Mueller one. The formalism based on 4×4 $\mathbf{Z}$ states that we developed recently [29,30] is particularly suitable for this kind of evaluation since it allows for a direct calculation. If we consider the system setup of Fig. 3 the superposition $\mathbf{Z}$ state reaching the detector is given by

$$\mathbf{Z}(x, y) = \frac{1}{\sqrt{2}}\mathbf{Z}_S\mathbf{Z}_H\mathbf{Z}_{45} + \frac{1}{\sqrt{2}}e^{i\phi(x,y)}\mathbf{Z}_S\mathbf{Z}_V\mathbf{Z}_{45} \tag{8}$$

where $\phi(x, y)$ is the phase difference at the detection plane (physically arising from the different optical paths of the ordinary and extraordinary beams) and $\mathbf{Z}_{45}, \mathbf{Z}_H, \mathbf{Z}_V$ are, respectively, the $\mathbf{Z}$ matrices of a polarizer with its transmission axis at 45°, a horizontal polarizer and a vertical polarizer [29]. $\mathbf{Z}_S$ represents the $\mathbf{Z}$ matrix of the sample.

When the birefringent crystal is oriented in such a way as the plane defined by the ordinary and extraordinary beams contains the horizontal or the vertical axis of the laboratory reference frame, the intensity pattern at the camera will exhibit vertical or horizontal fringes respectively (provided a dichroic sample is inserted into the recombined beam). In our experiment the crystal is oriented such that the plane defined by the two emerging beams contains the $y$ axis, so that we detect horizontal fringes; the intensity varies along the $y$ axis only. Equation (8) can be rewritten as:

$$\mathbf{Z}(y) = \mathbf{Z}_S\left[\frac{\mathbf{Z}_H}{\sqrt{2}} + \frac{e^{\phi(y)}}{\sqrt{2}}\mathbf{Z}_V\right]\mathbf{Z}_{45} = \mathbf{Z}_S\mathbf{Z}_R(y)\mathbf{Z}_{45} \tag{9}$$

where

$$\mathbf{Z}_R = \frac{1}{\sqrt{2}}\begin{pmatrix} 1+e^{i\phi} & 1-e^{i\phi} & 0 & 0 \\ 1-e^{i\phi} & 1+e^{i\phi} & 0 & 0 \\ 0 & 0 & 1+e^{i\phi} & -i(1-e^{i\phi}) \\ 0 & 0 & i(1-e^{i\phi}) & 1+e^{i\phi} \end{pmatrix}. \tag{10}$$

The Mueller matrix associated to this $\mathbf{Z}$ matrix is

$$\mathbf{M}_R(y) = \mathbf{Z}_R(y)\mathbf{Z}_R^*(y) = \begin{pmatrix} 1 & 0 & 0 & 0 \\ 0 & 1 & 0 & 0 \\ 0 & 0 & \cos\phi(y) & -\sin\phi(y) \\ 0 & 0 & \sin\phi(y) & \cos\phi(y) \end{pmatrix}, \tag{11}$$

which is the Mueller matrix of a horizontal linear retarder with retardation $\phi(y)$. Then the Mueller matrix of the entire system can be simply written as

$$\mathbf{M}(y) = \mathbf{Z}(y)\mathbf{Z}^*(y) = \mathbf{M}_S\mathbf{M}_R(y)\mathbf{M}_{45}, \tag{12}$$

Optics EXPRESS

where $\mathbf{M}_S$ is the Mueller matrix of the sample and $\mathbf{M}_{45}$ is the Mueller matrix of the polarizer oriented at 45°.

By using the Jones formalism it is likewise straightforward to verify that our double refracting crystal acts as a horizontal linear retarder. Indeed, it can be written as the coherent addition of a horizontal linear polarizer and a vertical linear polarizer with a phase difference:

$$\mathbf{J}_R(y) = \begin{pmatrix} 1 & 0 \\ 0 & 0 \end{pmatrix} + e^{i\phi(y)} \begin{pmatrix} 0 & 0 \\ 0 & 1 \end{pmatrix} = \begin{pmatrix} 1 & 0 \\ 0 & e^{i\phi(y)} \end{pmatrix}. \tag{13}$$

Finally, transforming the Jones matrix from Eq. (13) to a Mueller matrix again results in Eq. (11).

The light intensity at the detector is proportional to the first element of the Mueller matrix given by Eq. (12),

$$I(y) = (m_{00} + m_{02} \cos \phi(y) + m_{03} \sin \phi(y)) I_0, \tag{14}$$

where $m_{00}$, $m_{02}$ and $m_{03}$ are the elements of the Mueller matrix of the sample, $\mathbf{M}_S$, and $I_0$ is the intensity of the probing beam. This expression shows that a sample with non-vanishing $m_{02}$ or $m_{03}$ elements will produce spatial variation of the detected intensity. Note that the Stokes-Mueller analysis of commercial CD instruments is based on this same equation but with a temporal variation of the intensity instead of a spatial one.

## Funding

Ministerio de Economía y Competitividad (CTQ2017-87864-C2-1-P and EUIN2017-88598); European Commission (Polarsense, MSCA-IF-2017-793774).

## Acknowledgments

The authors are grateful to Dr. Enric Garcia-Caurel for helpful discussions.

## Disclosures

The authors declare that there are no conflicts of interest related to this article.

## References

1. N. Berova, K. Nakanishi, and R. Woody, *Circular dichroism: principles and applications* (Wiley-VCH, 2000).
2. O. Arteaga, J. Freudenthal, B. Wang, S. Nichols, and B. Kahr, "Circular dichroism with multiple photoelastic modulators," Chem. Today **30**, 6805–6817 (2012).
3. M. Grosjean and M. Legrand, "Polarimetrie. Appareil de mesure du dichroïsme circulaire dans le visible et l'ultraviolet," Compt. Rend. **251**, 2150–2152 (1960).
4. A. S. Alenin and J. S. Tyo, "Generalized channeled polarimetry," J. Opt. Soc. Am. A **31**, 1013–1022 (2014).
5. A. S. Alenin, I. J. Vaughn, and J. Scott Tyo, "Optimal bandwidth and systematic error of full-Stokes micropolarizer arrays," Appl. Opt. **57**, 2327–2336 (2018).
6. F. Gori, "Measuring Stokes parameters by means of a polarization grating," Opt. Lett. **24**, 584–586 (1999).
7. K. Oka and N. Saito, "Snapshot complete imaging polarimeter using Savart plates," Proc. Vol. 6295, Infrared Detect. Focal Plane Arrays VIII; p. 629508 (2006).
8. H. Luo, K. Oka, E. DeHoog, M. Kudenov, J. Schiewgerling, and E. L. Dereniak, "Compact and miniature snapshot imaging polarimeter," Appl. Opt. **47**, 4413–4417 (2008).
9. K. Oka and T. Kaneko, "Compact complete imaging polarimeter using birefringent wedge prisms," Opt. Express **11**, 1510–1519 (2003).
10. K. H. Nordsieck, "A Simple Polarimetric System for the Lick Observatory Image-Tube Scanner," Publ. Astron. Soc. Pac. **86**, 324–329 (1974).
11. K. Oka and T. Kato, "Spectroscopic polarimetry with a channeled spectrum," Opt. Lett. **24**, 1475–1477 (1999).
12. W. Sparks, T. A. Germer, J. W. MacKenty, and F. Snik, "Compact and robust method for full Stokes spectropolarimetry," Appl. Opt. **51**, 5495–5511 (2012).
13. P. Pagliusi, C. Provenzano, A. Mazzulla, L. Giorgini, and G. Cipparrone, "Spectrograph Based on a Single Diffractive Element for Real-Time Measurement of Circular Dichroism," Appl. Spectrosc. **62**, 465–468 (2008).

Optics EXPRESS


14. C. Provenzano, P. Pagliusi, A. Mazzulla, and G. Cipparrone, "Method for artifact-free circular dichroism measurements based on polarization grating," Opt. Lett. **35**, 1822–1824 (2010).
15. M. Terazima, "A New Method for Circular Dichroism Detection Using Cross-Polarized Transient Grating," The J. Phys. Chem. **99**, 1834–1836 (1995).
16. M. W. Kudenov, M. J. Escuti, N. Hagen, E. L. Dereniak, and K. Oka, "Snapshot imaging Mueller matrix polarimeter using polarization gratings," Opt. Lett. **37**, 1367–1369 (2012).
17. O. Arteaga, R. Ossikovski, E. Kuntman, M. A. Kuntman, A. Canillas, and E. Garcia-Caurel, "Mueller matrix polarimetry on a Young's double-slit experiment analog," Opt. Lett. **42**, 3900–3903 (2017).
18. F. Arago and A. J. Fresnel, "On the action of rays of polarized light upon each other," Ann. Chim. Phys. **2**, 288–304 (1819).
19. M. Mujat, A. Dogariu, and E. Wolf, "A law of interference of electromagnetic beams of any state of coherence and polarization and the Fresnel-Arago interference laws," J. Opt. Soc. Am. A **21**, 2414–2417 (2004).
20. R. Ossikovski, O. Arteaga, J. Vizet, and E. Garcia-Caurel, "On the equivalence between Young's double-slit and crystal double-refraction interference experiments," J. Opt. Soc. Am. A **34**, 1309–1314 (2017).
21. G. Lambert, B. Vodungbo, J. Gautier, B. Mahieu, V. Malka, S. Sebban, P. Zeitoun, J. Luning, J. Perron, A. Andreev, S. Stremoukhov, F. Ardana-Lamas, A. Dax, C. P. Hauri, A. Sardinha, and M. Fajardo, "Towards enabling femtosecond helicity-dependent spectroscopy with high-harmonic sources," Nat. Commun. **6**, 6167 (2015).
22. J. Meyer-Ilse, D. Akimov, and B. Dietzek, "Ultrafast Circular Dichroism Study of the Ring Opening of 7-Dehydrocholesterol," The J. Phys. Chem. Lett. **3**, 182–185 (2012).
23. A. Trifonov, I. Buchvarov, A. Lohr, F. Würthner, and T. Fiebig, "Broadband femtosecond circular dichroism spectrometer with white-light polarization control," Rev. Sci. Instruments **81**, 043104 (2010).
24. A. Ferré, C. Handschin, M. Dumergue, F. Burgy, A. Comby, D. Descamps, B. Fabre, G. A. Garcia, R. Géneaux, L. Merceron, E. Mével, L. Nahon, S. Petit, B. Pons, D. Staedter, S. Weber, T. Ruchon, V. Blanchet, and Y. Mairesse, "A table-top ultrashort light source in the extreme ultraviolet for circular dichroism experiments," Nat. Photonics **9**, 93–98 (2014).
25. T. Mu, C. Zhang, Q. Li, L. Zhang, Y. Wei, and Q. Chen, "Achromatic Savart polariscope: choice of materials," Opt. Express **22**, 5043–5051 (2014).
26. J. Schellman and H. P. Jensen, "Optical spectroscopy of oriented molecules," Chem. Rev. **87**, 1359–1399 (1987).
27. O. Arteaga, "Mueller matrix polarimetry of anisotropic chiral media," Ph.D. thesis, University of Barcelona (2010).
28. O. Arteaga, J. Freudenthal, B. Wang, and B. Kahr, "Mueller matrix polarimetry with four photoelastic modulators: theory and calibration," Appl. Opt. **51**, 6805–6817 (2012).
29. E. Kuntman, M. Ali Kuntman, and O. Arteaga, "Vector and matrix states for Mueller matrices of nondepolarizing optical media," J. Opt. Soc. Am. A **34**, 80 (2016).
30. E. Kuntman, M. A. Kuntman, J. Sancho-Parramon, and O. Arteaga, "Formalism of optical coherence and polarization based on material media states," Phys. Rev. A **95** (2017).